Journal of Cleaner Production 519 (2025) 146044

Contents lists available at ScienceDirect

Journal of Cleaner Production

journal homepage: www.elsevier.com/locate/jclepro

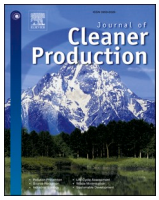

Mechanical performance of sustainable composite material: Wet-laid and dry-laid nonwoven textiles made out of recycled carbon fibers with thermoset and thermoplastic matrices

Fabian Rechsteiner [a,*], Luca Raimondi [b], Nicola Tegas [a], Lorenzo Donati [b], Frank Manis [a]

[a] Fraunhofer Institute for Casting, Composite and Processing Technology, Augsburg, Germany
[b] DIN – Department of Industrial Engineering, Viale risorgimento 2, 40139, Bologna, Italy

ARTICLE INFO

Keywords:
Dry-laid
Wet-laid
Recycled carbon fiber
Compression molding
Sustainable thermoset composites
Sustainable thermoplastic composites

ABSTRACT

The utilization of recycled carbon fibers (rCF) in thermoplastic and thermoset composites shows significant potential in terms of economic and ecological benefits. rCFs offer a cost-effective alternative to virgin fibers with savings in energy and resources, contributing to a better ecological performance of the material. Currently, there is limited knowledge on the mechanical performance of non-wovens out of rCF. Therefore, this study uses production waste of virgin carbon textiles to investigate the mechanical properties of rCF composite materials utilizing two distinct nonwoven manufacturing techniques (dry-laid and wet-laid). The textiles are each combined with two different polymers: a thermoplastic PA66/6I and a thermosetting polymer based on an epoxy resin. Following this, three different characterization tests, following ASTM standards, analysing different mechanical properties are carried out: tensile, flexural, and compressive. Optical analysis was conducted to assess the impregnation quality of the fibers and the matrix as well as a fiber volume determination through wet-chemical analysis. Mechanical tests show that dry-laid -nonwovens have high, repeatable stiffness (18–28 GPa) across all stress modes and superior cross-direction performance due to carding, while wet-laid-nonwovens offer uniform stiffness (16–26 GPa) with more isotropic behavior.

1. Introduction

To meet the growing demand for lightweight, energy-efficient products and reduce vehicle energy consumption, modern industries have increasingly turned to composite materials, particularly carbon fiber reinforced plastics (CFRPs), due to their exceptional mechanical properties, lightweight nature, and design flexibility (Ahmad et al., 2020; Almushaikeh et al., 2023; Hsissou et al., 2021; Joost, 2012). While CFRPs offer attractive benefits, their energy-intensive production and disposal raise significant environmental concerns (Danish et al., 2022; Iyer et al., 2024). With the large and rapidly expanding market for CFRPs (Witten Elmar and Volker Mathes, 2022), there is a pressing need for effective recycling technologies and a deeper understanding of the properties of materials made from recycled carbon fibers (rCFs). Using recycled materials has numerous benefits, such as waste reduction, resource conservation, the promotion of a circular economy, and, foremost, the reduction of energy usage and greenhouse gas emissions. Especially the needed energy to produce virgin Carbon Fibers (vCF) is fairly high and this energy consumption can drastically be reduced by increasing the use of (rCFs) (Gopalraj et al., 2021; Vo Dong et al., 2018). The production of vCF necessitates an energy input ranging from 464 to 704 MJ/kg (Das, 2011; Prenzel et al., 2024), whereas the recycling of CFRP requires significantly less energy, with consumption levels varying between 2.03 MJ/kg and 30 MJ/kg, depending on the recycling process (Howarth et al., 2014; Witik et al., 2013).

Three primary sources (Heidarian et al., 2024) contribute to waste carbon fibers: (i) reclaimable carbon fibers from End-of-Life (EoL) products, (ii) prepreg residues and semi-finished products, and (iii) carbon fiber offcuts. The field of recycling and reclaiming carbon fiber composites is still in its early stages of research, but it has seen noteworthy advancements in the last twenty years. Reclamation and recycling techniques for EoL products can be classified into three main categories, each with its advantages and limitations: mechanical (Khurshid et al., 2020), thermal (including pyrolysis (Naqvi et al., 2018) and fluidized bed (Oliveux et al., 2015)), and chemical recycling (De Fazio et al., 2023; Kim and Kim, 2023). In addition to the limited EoL

* Corresponding author.
E-mail address: fabian.rechsteiner@igcv.fraunhofer.de (F. Rechsteiner).

https://doi.org/10.1016/j.jclepro.2025.146044
Received 12 December 2024; Received in revised form 18 June 2025; Accepted 21 June 2025
Available online 1 July 2025

reclamation options, carbon fiber offcuts account for up to 40 % of textile waste generated as production scrap due to cutting and discarding during manufacturing (Meng et al., 2018; Shen et al., 2023), usually fractioned, landfilled, or incinerated resulting in a loss of the energetic value of the material. These fibers are valuable because they remain identical to virgin carbon fibers (vCF), having not undergone any thermal or chemical processes that could degrade their properties (Badrul Hasan et al., 2019). They also serve as a benchmark for recycling processes, as the most effective method preserves the original material's chemical and physical characteristics. Due to processing requirements, the rCF usually exists not in endless but short fiber lengths below 100 mm. Up to this point, the fibers cannot be used to produce conventional textiles such as non-crimp fabrics, wovens, or even rovings and be processed in typical FRP manufacturing processes. As a result, only a few modified textile technologies, including dry-laid (DL) carding and wet-laid (WL), can produce textile preforms from these short fibers for reuse in the composites industry (Barnett and Ghossein, 2021). Carding can be divided into five steps: (i) feeding, (ii) carding, (iii) web formation, (iv) cross-lapping, and (v) needle punching. During feeding, the short fibers (40 mm–100 mm) are fed into the carding machine, opened, and separated from each other through a constant flow of air. In the next step, the material is carried on the carding rollers, where the fibers are aligned and combed into the direction of production (0°). This work is being done through fine wire teeth of the carding rollers moving in one direction and workers and strippers moving in the opposite direction, giving the fibers an orientation at 0°. The fibers are then collected and form a web on a conveyor belt. This web is then cross-lapped in a 90° direction onto another conveyor belt, where the number of web layers determines the aerial weight of the nonwoven. Due to this cross-lapping in a 90° direction, the material has a slight orientation in the transverse direction. As a final step, the material is penetrated with a board of needles moving up and down at a high speed, which entangles the fibers and gives the fabric strength and stability (Handbuch Faserverbundkunststoffe/Composites, 2013; Henning and Moeller, 2020). A schematic illustration of the carding process is displayed in Fig. 1.

The production of WL nonwoven is similar to the papermaking process and can be divided into three steps: (a) preparation and dispersion, (b) web formation, and (c) dewatering and drying. In the first steps, the fibers (~3 ÷ 18 mm long) are fed into water and singled out through high shear forces. Through pipes, the fiber-water suspension is transferred onto a rotating sieve belt through a rotary distributor. Here, the web is formed, and the water is removed through pumps underneath the sieve belt. In the final step, the material is dried in an oven (Cherif, 2011). Fig. 2 presents a picture of an industrial-scale WL machine divided into the three production steps described.

Both of these technologies are used to produce nonwovens but currently have limited usage in the field of rCF (Barnett and Ghossein, 2021). It is well established in the literature that nonwoven composites can exhibit varying degrees of anisotropy based on the manufacturing process adopted to manufacture dry preforms. WL or air-laid techniques generally produce isotropic textiles, ideal for thin, in-plane-loaded applications. In contrast, carding or yarn-spinning techniques generally produce anisotropic textiles as fibers tend to be mostly aligned in a preferential direction. Similar to traditional continuous fiber composites, these anisotropic composites require careful consideration of load conditions and laminate sequencing, yet they offer a potential for greater cost and weight reductions compared to isotropic textiles (David et al., 2023). Distinct manufacturing routes were explored in the literature to produce composites out of nonwoven textiles composed by rCF, using both thermoplastics (TPs) and thermosetting (TS) polymers as matrices. Hot pressing and compression molding are well-established techniques to manufacture TP composites from DL (Manis et al., 2021; Rimmel et al., 2019; Xiao et al., 2019) and WL (Barnett et al., 2021; Pimenta et al., 2010; Wong et al., 2014) textiles. In the literature, the highest tensile modulus and strength were obtained using PA6 and PA66 as reinforcement matrices at a typical fiber volume content (FVC) of about 30 % (Barnett and Ghossein, 2021). In contrast, Resin Transfer Molding (RTM), autoclave, and wet compression molding have been successfully utilized to produce TS composites from DL and WL nonwovens (David et al., 2023; Feraboli et al., 2012; Genna et al., 2020; Shah and Schubel, 2016). Epoxy was the most used TS resin due to its high-quality impregnation and favourable surface chemistry with staple fibers. However, FVC hardly exceeds 40 % due to the formation of voids and other impregnation defects. In the current state-of-the-art, the mechanical characterization data from rCF composites is insufficient for comprehensive benchmark analysis. Most of these composites are assumed to exhibit random fiber orientation; however, many studies have not tested samples in orthogonal directions to validate this assumption. Additionally, fiber dispersion in the microstructure, which significantly affects tensile strength, is often overlooked. Unfortunately, there is limited information in the literature regarding the compression properties of carded textile composites made from recycled carbon fibers (Barnett and Ghossein, 2021). Manis et al. (2021), Wan et al. (Wan and Takahashi, 2016) and Shao et al. (Fu et al., 2019) have investigated the flexural and tensile properties of thermoplastic rCF composites from carded nonwoven, leaving thermoset polymers and WL nonwovens less explored. Sauer (Sauer et al., 2019) explored the tensile and bending properties of thermoplastic WL nonwoven composites while leaving thermoset polymers unaddressed. While a study from Wölling (Wölling et al., 2017) has assessed the difference between dry- and WL nonwovens, a gap still exists in the compressive strengths of these materials as well as a deep microstructural analysis. Moreover, only a minority of

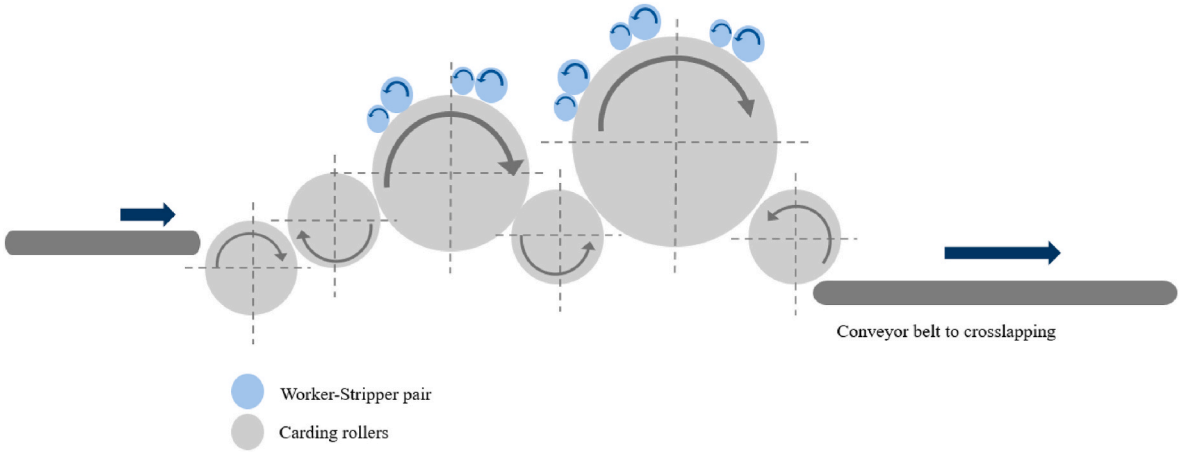

Fig. 1. Simplified, schematical visualization of the carding part of the dry-laid nonwoven machine, adapted from (Manis et al., 2021).

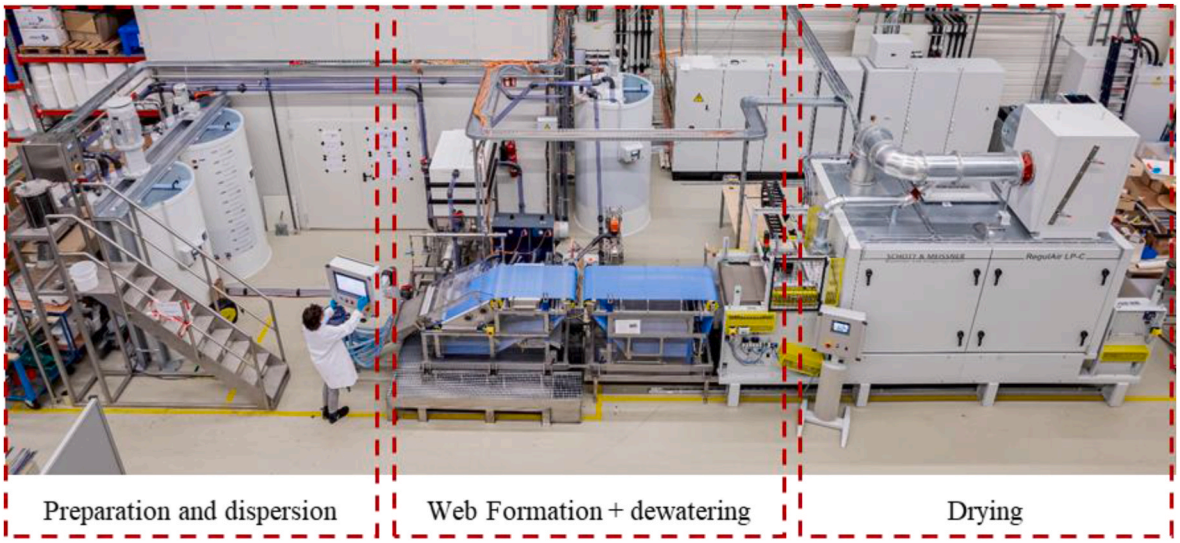

Fig. 2. Overview of the wet-laid nonwoven plant at Fraunhofer IGCV. © A3 | Christian Strohmayr

studies encompass both tensile and compressive testing methodologies; those incorporating both are frequently constrained to examining particular materials, thereby hindering the ability to extend the results across diverse textiles or matrix systems. In contrast to prior studies, in this work high-performance reclaimed nonwoven carbon fabric is used to produce CFRP laminates by compression molding technology. To assess their suitability for automotive use, the mechanical behavior of the developed materials is benchmarked using lightweight material selection indices—specifically stiffness-to-weight, strength-to-weight, bending stiffness ($\sqrt[3]{E}/\rho$), and buckling resistance ($\sqrt{E}/\rho$) —which are widely applied in material selection for structural and panel components ((BMW), 1999; Cui et al., 2011; Sun and Tao, 2018). Two distinct nonwoven manufacturing techniques —DL and WL— were employed, combining the fabrics with both thermoplastic (PA66/6I) and thermoset (epoxy) matrices to evaluate their mechanical performance. By integrating optical microscopy and chemical analysis to assess fiber impregnation quality and fiber volume content, this study advances current understanding of rCF composite material behavior. Unlike previous studies, this work performs an extensive characterization campaign (tensile, compression and flexural) to evaluate the fundamental mechanical properties of each material and provide deeper insights of material behaviour under different loading conditions.

2. Materials and methods

2.1. Materials

Two types of nonwovens are adopted, both processed using carbon fibers derived from dry textile cut-offs. One nonwoven was processed through the DL carding line from Tenowo (Hof, Germany) using Mitsubishi Pyrofil™ HR carbon fibers up to ~100 mm in length. The second nonwoven was a WL textile from Marubeni International (Düsseldorf, Germany), consisting of ~6–10 mm of Toray® (Tokyo, Japan) T-700 Standard Modulus Carbon Fibers. Grammage of both textiles was 100 g/m^2 (averaged, as supplied). Fig. 3 shows the described DL and WL nonwoven fabrics (0° and 90° indicate the machine and transverse directions, respectively).

As polymeric matrices, a thermoset (TS) epoxy resin system (Araldite LY3585/Aradur 3475) supplied by Huntsman Advanced Materials (Bergkamen, Germany), and a thermoplastic (TP) PA66/6I matrix supplied by Asahi Kasei Corporation were used in this study. Both materials' properties can be taken from Table 1.

The epoxy system consists of bisphenol-A-diglycidylether as the resin and a mixture of 1,3-cyclohexanedimethanamine and methyldiethanolamine as hardeners. This resin is widely applied in the mass production of automotive components for its short cure cycles and a

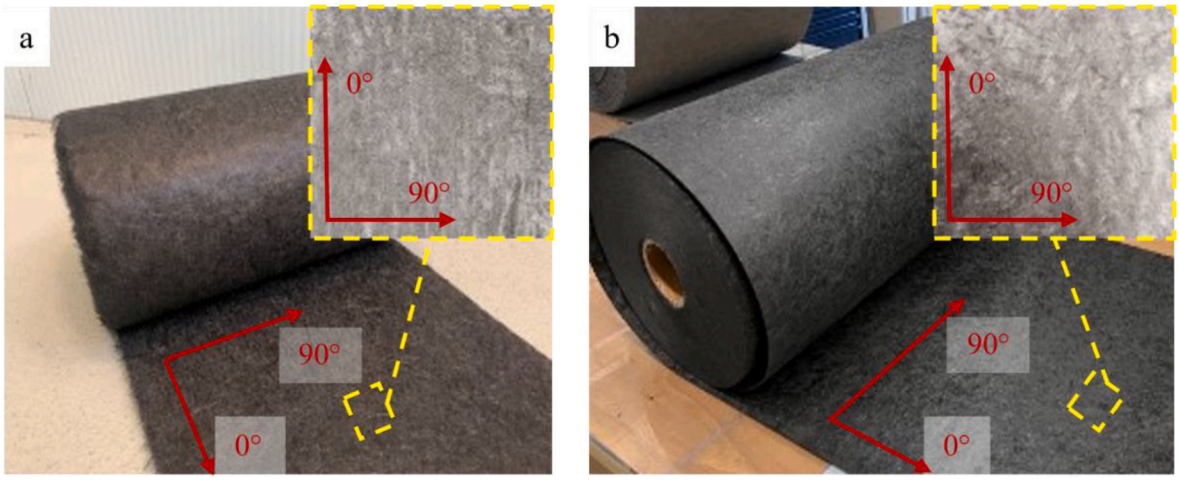

Fig. 3. Nonwoven fabrics a) Dry-laid nonwoven fabric. b) Wet-laid nonwoven fabric.

Table 1
Properties of the polymeric matrix systems used.

	Epoxy	PA66/6I
Density (kg/m^3)	1140	1140
Glass transition temperature (°C)	120	89
Melting temperature (°C)	–	222
Tensile strength (MPa)	75	83
Tensile modulus (GPa)	2.7	2.7

glass transition temperature of about 120 °C (Zweifel and Brauner, 2020). The thermoplastic material was supplied as a powder with an average particle size of 100 μm and is under development by the supplier, especially for short-fiber textiles. The physical properties of both TS and TP resins are reported in Table 1.

2.2. Processing of nonwovens

The production method selected for the thermoset materials was wet compression molding, while hot-pressing was used for the thermoplastic material. Both processes were carried out using a specifically designed 350 mm × 500 mm heatable and coolable steel mold installed into a 130 t LZT-OK-130L hydraulic press from Langzauner GmbH, as shown in Fig. 4a.

The process began by cutting the nonwoven fabric into patches measuring 350 mm × 500 mm to ensure complete mold coverage. Before processing, the textile layers were conditioned in an oven and dried at 80 °C for 2 h to remove any moisture. The Araldite polymer was mixed with the hardener (100:21 wt ratio) as suggested by the manufacturer, then placed in a vacuum degassing system for 5 min to eliminate any trapped air. Before placing the materials in the mold, the polymeric matrix was directly applied to each layer of the TP material and every fourth layer of the TS material. Care was taken to distribute the matrices evenly to mitigate the formation of voids or resin pockets in subsequent manufacturing phases. Distinct processing routes were adopted to manufacture TP and TS plates. To manufacture the TS material, both halves of the mold were heated at 130 °C and monitored through thermocouples with a tolerance of 5 °C; the stacked nonwovens with TS polymer was positioned in the mold (Fig. 4b), and the resin was cured for 5 min at a pressure of 20 bar. To manufacture the TP material, the stacked nonwoven with distributed TP material (Fig. 4b) were compressed at 5 bars and heated from room temperature to 290 °C following a ramp of 10 °C per minute to allow PA66/6I to melt. When the temperature was reached, the material was pressed at 40 bar to the intended 2 mm thickness. At the end of the consolidation step, both TS and TP plates were cooled down at room temperature through the mold, extracted, and visually checked for imperfections. Fig. 4c shows a panel after compression molding. To facilitate demoulding, a PAT®-527/2 release agent (E. und P. Würtz GmbH & Co. KG, Bingen am Rhein, Germany) was applied over the tool. For each material combination, at least 3 panels were produced. An overview of the different material combinations, the averaged dry stack weight, and the averaged values from manufactured plates are reported in Table 2.

2.3. Fiber volume content and microsection

Wet chemical solvolysis, as per DIN EN 2564, was carried out to determine the fiber volume content of the produced materials. For this test three specimen from each material are used with a weight of approximately 2g. The matrix was dissolved by boiling the samples at an approximate temperature of 170 °C in 98 % concentrated sulfuric acid for 1 h, followed by the addition of 30 % hydrogen peroxide. After dissolution, fibers were filtered out, rinsed, and dried for 2 h at 120 °C in an oven. The weight of the dried fibers was compared with the initial sample weight to calculate the fiber volume content. Even though, this analysis is standardised and is not prone to error, inaccuracies in test results may occur due to incomplete resin dissolution or different moisture contents in the specimen. For the optical analysis of the microsections, specimens from the bending test were embedded in a resin system KEM Qpox 90 (ATM Qness GmbH, Mammelzen, Germany) and cured for 24 h. The embedded specimens were then wet grounded using SiC paper with decreasing grain size (320 μm, 600 μm, and 1200 μm) with constant addition of water. The test disc holding the embedded specimen rotated at 150 rpm in the same direction as the working disc at 100 rpm. The surface of the samples was then polished in a five-stage process with the addition of diamond suspension with decreasing grain size (9 μm, 6 μm, 3 μm, 1 μm, 0.06 μm) to achieve a clean and scratch-free surface. The optical analysis was performed using an incident light contrast microscope (Leica DM 4000) with a maximum magnification of 100 × .

2.4. Mechanical characterization of rCF nonwovens

2.4.1. Tensile properties

Tensile tests were performed using a properly calibrated Zwick/Roell universal testing machine (Z050) equipped with a 50 kN load cell. The tests were conducted in displacement control at a constant crosshead speed of 2 mm/s, per ASTM D3039. An extensometer with a gauge length of 50 mm was used to measure deformations. Five samples of each material type, measuring 250 mm × 50 mm, were extracted from panels in both the machine direction (0°) and transverse direction (90°)

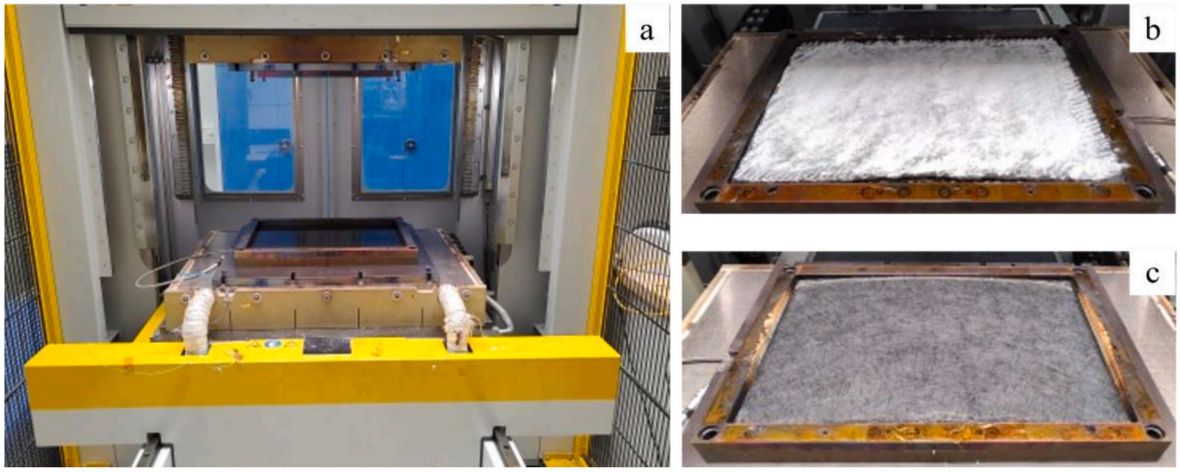

Fig. 4. Equipment and materials used for nonwoven processing. a) Langzauner hydraulic press with heatable and coolable mold b) TP material charge in the mold before hot pressing c) TS charge in the mold before compression molding.

Table 2
Overview of the different material combinations and averaged values from manufactured plates.

Material	Textile	Stack weight [g]		Matrix	Matrix weight [g]		Thickness [mm]		Panel weight [g]	
		Avg.	StDev		Avg.	StDev	Avg.	StDev	Avg.	StDev
DL-TS	DL	208.83	16.27	TS	430	0.01	2.35	0.19	525.48	39.56
WL-TS	WL	184.98	2.48	TS	360	0.01	2.71	0.40	552.23	14.34
DL-TP	DL	220.85	29.16	TP	349	0.01	2.51	0.25	578,67	46.45
WL-TP	WL	224.93	3.19	TP	349	0.01	2.44	0.05	569.67	4.98

using a high-speed rotating saw disk. The clamping distance was 50 mm. Emery cloth was placed between the grips and the coupons to prevent slippage.

2.4.2. Compressive properties

Compressive tests were conducted according to ASTM D3410, with a 1.5 mm/min crosshead displacement speed. Five samples of each material type were taken from molded panels in both the 0° and 90° directions using a high-speed rotating saw disk. The specimens, measuring 140 mm × 25 mm, were clamped over a length of 65 mm on both edges. Cap strips were glued onto the specimen to avoid breakage in the clamping area. Strain gauges with an active grid length of 4 mm were employed to monitor secondary bending and measure the compressive modulus.

2.4.3. Flexural properties

The flexural properties of the samples were assessed according to ASTM D790 through a three-point bending test procedure. A constant span-to-thickness ratio of 1/32 was employed throughout the experiments, while a 10 kN load cell was used to measure the force. Five specimens were prepared and tested for each type of material produced in both the 0° and 90° orientations.

2.4.4. Statistical analysis

The mechanical properties of the tested materials were analyzed using statistical validation to determine whether the observed differences were statistically significant or merely experimental variations. Given the small sample size (n = 5 per group) and the potential presence of variance differences across groups, Welch's T-Test was selected as the most appropriate method for comparing the properties of each material combination (Rietveld and van Hout, 2015). To further support the findings, Hedges' g effect size was calculated to measure the practical significance of differences between groups. A significance threshold of $p < 0.05$ was used for Welch's T-Test, and effect sizes were interpreted using standard benchmarks ($g > 0.8$ indicating a significant effect). All statistical analysis was conducted using Python's SciPy and Statsmodels libraries (Seabold and Perktold, 2010).

2.4.5. Assessment for application in the automotive sector

To evaluate the suitability of the investigated rCF materials for automotive structural and semi-structural applications, a performance-based assessment was carried out using established material selection indices and benchmarked against data from a commercial automotive-grade SMC (Falaschetti et al., 2024; Martulli et al., 2020; Falaschetti et al., 2025a). For frame components, the analysis considered membrane stiffness efficiency from Young Modulus E and density ρ (Eq. (1))

$$E/\rho \tag{1}$$

buckling resistance efficiency, using the ultimate strength R in compression (Eq. (2))

$$\sqrt{R}/\rho \tag{2}$$

and specific strength as per Eq. (3)

$$R/\rho \tag{3}$$

while for body panels, the specific bending stiffness Eq. (4)

$$\sqrt[3]{E_f}/\rho \tag{4}$$

The specific buckling stiffness Eq. (5)

$$\sqrt{E_f/\rho} \tag{5}$$

and flexural specific strength (6)

$$R_f/\rho \tag{6}$$

were evaluated, using the flexural modulus E_f and flexural strength R_f. All parameters were computed using the minimum and maximum values of tensile, compressive, and flexural properties obtained in both principal orientations (0° and 90°), thereby capturing the anisotropic response of the laminates. This index-based approach permits a direct, function-specific comparison with existing industrial benchmarks and highlights the potential of rCF systems to satisfy application-driven requirements following well-established material selection protocols ((BMW), 1999).

2.5. Fractured surfaces and morphological characterization analysis

The fractured surfaces of the tensile samples were initially analyzed using a Stereo Microscope (ZEISS Stemi 508 Greenough equipped with a 5 MP ZEISS Axiocam 105 color camera) to investigate their macroscopic in-plane failure behavior after testing. The morphological fracture modes were further assessed via Scanning Electron Microscopy (SEM, Phenom ProX) for cross-section analysis. To make the surfaces conductive, they were gold-coated.

3. Results and discussion

3.1. Fiber volume content and microsection

Table 3 shows each material combination's fiber volume and mass content (FVC/FMC). The aimed FVC was 30 %, almost reach for DL-TS, DL-TP, and WL-TP materials with 28.02 %, 28.21 %, and 27.47 %, respectively. Only material WL-TS had a lower FVC of 22 %. Signific higher mechanical properties could be expected if a similar high FVC could be reached with material WL-TS.

To understand the impregnation quality and potential voids inside

Table 3
Fiber volume/mass content of the different material combinations with the corresponding standard deviation.

Material	FVC [%]		FMC [%]	
	Avg.	St. Dev.	Avg.	St. Dev.
DL-TS	28.02	1.18	39.54	1.75
WL-TS	22.70	0.24	31.75	0.08
DL-TP	28.21	1.02	37.46	1.17
WL-TP	27.47	0.23	36.58	0.26

the material, specimens of all materials have been polished and investigated with a transmitting light microscope.

The microstructure of DL-TS and WL-TS materials at 0° can be seen in Fig. 5 and a higher scaling factor in Fig. 6. By comparing both thermoset materials with the different nonwoven manufacturing techniques, it can be seen in Fig. 5a that the DL nonwoven shows fewer but bigger voids in the composite material. The WL shows more, smaller, and more evenly distributed voids throughout this microsection, as illustrated in Fig. 5b. It can also be seen that the DL material shows a less opened fiber due to the textile processing. The fiber bundle opening within the WL processing is much higher, and the fibers are, therefore, strongly separated from each other. This leads to local fiber bundles and matrix rich regions within the DL material what may influence the mechanical performance.

Fig. 7 shows the microsection of DL-TP and WL-TP materials, both manufactured with thermoplastic PA66/6I matrix. It is evident that both materials exhibit fewer and smaller voids within the composite material compared to TS, indicating effective impregnation of the polymer with the fibers. The fiber footprint from micrographic images appears mainly elliptical for all materials, with major and minor axes varying from fiber to fiber. WL materials (Figs. 6b–8b) exhibit numerous fibers of circular shape, while DL materials (Figs. 6a–8a) exhibit fiber footprints that are always elliptical, some with abnormally large major axes. Considering that the elliptical footprint of fibers is closely associated with their orientation (Raimondi et al., 2021; Yurgartis, 1987), it can be concluded that DL materials exhibit a more pronounced alignment in the 90° direction than WL materials. The reason for the higher alignment in 90° from the DL materials may lie in the production of the carded DL textile. At the beginning of the process, the fibers are carried in the direction of production, and after this carding and web formation step, the material is cross-lapped at 90° to the production direction, which gives the material a slight orientation towards 90°. Similar to the TS materials, more fiber bundles are visible in the DL-material (Figs. 6a and 8a) than in the WL-material (Figs. 6b and 8b) due to their different nonwoven manufacturing technologies, which could influence mechanical properties. In the WL technology, the material experiences a more thorough fiber opening process, leading to a better distribution of the fibers in the nonwoven.

3.2. Mechanical characterization of rCF nonwovens

3.2.1. Tensile properties

The self-measured tensile response of the composites is summarized in Table 4 and visualized in Fig. 9.

Good repeatability of Young's modulus was observed across all samples, with coefficient of variation (CV) values consistently below 7 %. As illustrated in Fig. 9a, the DL-TS material exhibits a linear elastic response at both 0° and 90°. Statistical analysis confirmed a significant increase in tensile modulus from 18.79 GPa at 0° to 26.47 GPa at 90° ($p < 0.00001$), indicating a higher stiffness in the cross direction, which suggests anisotropic behavior. T-test results confirmed a significant increase in ultimate tensile strength from 238.78 MPa at 0° to 308.10 MPa at 90° ($p < 0.00001$), further reinforcing the anisotropic behavior of DL-TS. Evaluations confirmed a slight but significant difference in strain to failure, with 1.19 % at 0° and 1.15 % at 90° ($p = 0.041$), indicating marginally better elongation in the machine direction. In contrast, Fig. 9b shows that WL-TS exhibits a more balanced behavior between 0° and 90°. However, statistical analysis confirmed a significant difference in tensile modulus: it is higher at 0° (20.74 GPa) than at 90° (18.03 GPa) ($p < 0.00001$), indicating mild anisotropy. However, the average tensile strength values (337.18 MPa at 0° vs. 273.64 MPa at 90°) were not statistically different ($p = 0.235$), suggesting that the material maintains similar strength across orientations. Likewise, strain-to-failure values (1.58 % at 0° vs. 1.54 % at 90°) were not significantly different ($p = 0.263$), confirming that the material deforms similarly in both directions. For DL-TP, Fig. 9c reveals a notable difference in stiffness between orientations ($p = 0.038$). The ultimate tensile strength follows a similar pattern, with much higher values at 90° (311.32 MPa, St.Dev.: 7.19 MPa) than 0° (165.58 MPa, St.Dev.: 37.41 MPa). The results from the T-test confirmed that the difference is significant ($p = 0.031$), which reinforces the anisotropic behavior of DL-TP. The strain to failure is higher at 90° (1.08 %, standard deviation: 0.05 %) compared to 0° (0.90 %, standard deviation: 0.20 %). However, the larger standard deviation at 0° indicates greater variability in that direction. Despite this, a quantitative assessment shows that this difference is not significant ($p = 0.124$), suggesting that the variability at 0° does not imply a fundamental difference in mechanical properties. Fig. 9d shows that WL-TP displays more uniform properties between orientations. The average modulus at 0° is 25.56 GPa and slightly lower at 90° (23.88 GPa), indicating a fairly balanced stiffness, but the observed differences are within experimental variability ($p = 0.121$ for modulus, $p = 0.754$ for strength), confirming the material's isotropic nature. The tensile strength is higher at 90° (231.20 MPa) than at 0° (186.66 MPa), but the large St.Dev. values indicate significant variability. It's important to note that the fibers in the WL material are significantly shorter than those in the DL material. This shorter fiber length likely contributes to the higher variability in strength, as it may reduce the efficiency of load transfer and result in weaker bonding between the fibers and the matrix. The strain to failure is much higher at 90° than at 0°, reflecting more ductility in the cross direction. The reason for the higher performance in 90° from the DL materials lies in their microstructural properties as observed in Section 2.3. In conclusion, all materials present adequate properties compared with other short-fiber reinforced composites (S. J. Pickering et al., 2016; Zhao et al., 2018), and are even stronger than conventional materials widely used in automotive applications actually produced with virgin carbon fibers (Falaschetti et al., 2024), while small deviations exist between the textile and polymer types. The overall best

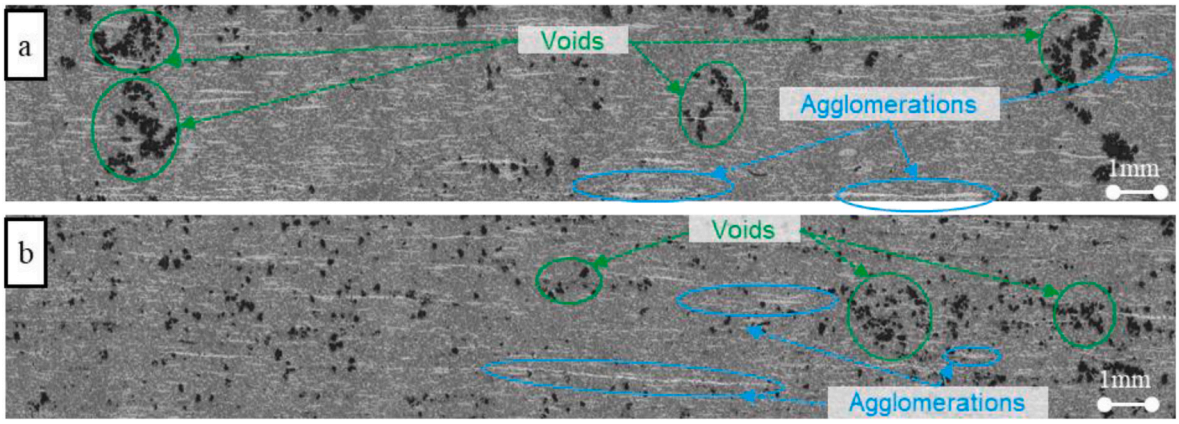

Fig. 5. Overview of internal microstructure of TS materials. a) DL-TS b) WL-TS.

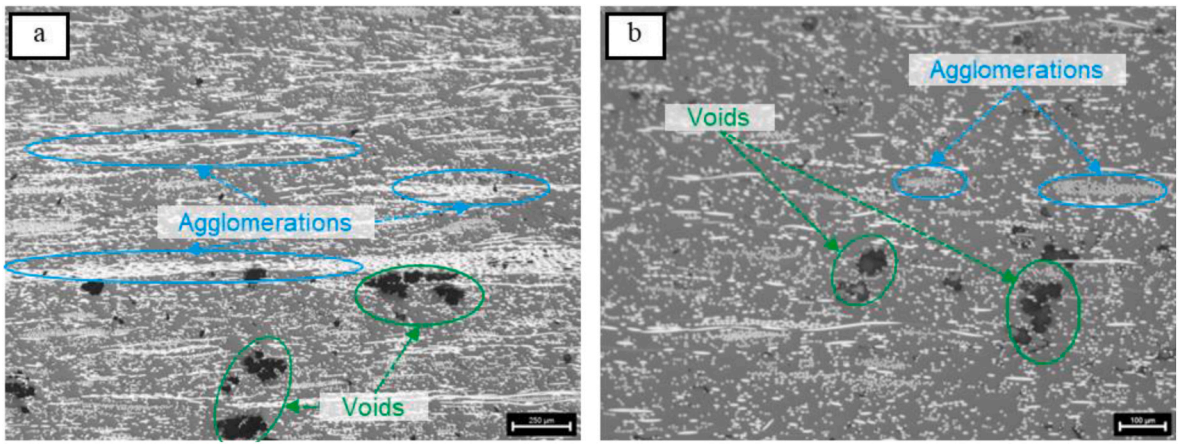

Fig. 6. Internal microstructure of TS materials. a) DL-TS b) WL-TS.

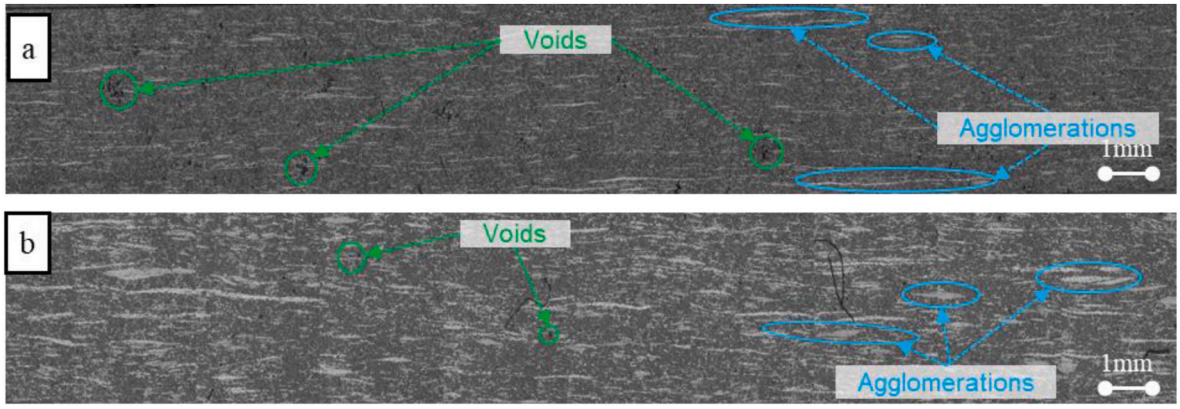

Fig. 7. Internal microstructure of TP materials. a) DL-TP b) WL-TP.

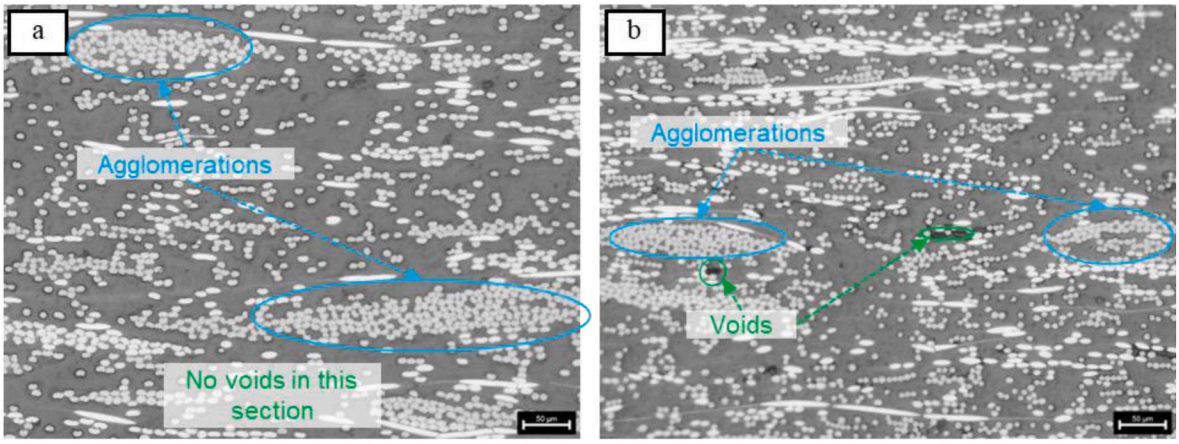

Fig. 8. Internal microstructure of TP materials. a) DL-TP b) WL-TP.

tensile performance is shown by WL textile and thermoplastic matrix.

3.2.2. *Compressive properties*

Self-measured compressive test results are detailed in Table 5 and represented in Fig. 10. Higher repeatability in modulus, ultimate strength, and strain to failure were observed across all materials, with the respective CV values consistently below 10 %.

A noticeable and consistent trend characterized the mechanical response of the different materials in compression. All the stress-strain curves follow a similar path: an initial linear elastic region, followed by a non-linear deformation phase, culminating in failure, as documented in Fig. 10a and d. Similarly to what was observed in Section 2.4.1, both DL-TS (Fig. 10a) and DL-TP (Fig. 10c) materials were stiffer in the cross direction than in the machine direction within the initial linear elastic region. This trend is reinforced by significant differences in compressive modulus ($p = 0.0022$ for DL-TS, $p < 0.00001$ for DL-TP), confirming their anisotropic behavior. Conversely, both WL-TS (Fig. 10b) and WL-TP (Fig. 10d) materials consistently exhibited

Table 4
Self-measured tensile properties of produced materials along different orientations.

Material	Angle	Modulus [GPa]		Strength [MPa]		Strain to Failure [%]	
		Avg.	St. Dev.	Avg.	St. Dev.	Avg.	St. Dev.
DL-TS	0°	20.0	1.0	238.78	7.13	1.19	0.02
	90°	25.6	0.6	308.10	9.87	1.15	0.07
WL-TS	0°	21.4	0.3	337.18	8.76	1.58	0.03
	90°	18.0	0.3	273.64	10.53	1.54	0.09
DL-TP	0°	22.9	0.8	166.00	37.00	0.90	0.20
	90°	28.0	4.0	311.00	7.00	1.08	0.05
WL-TP	0°	27.7	5.1	223.99	139.02	0.79	0.40
	90°	24.6	0.6	275.99	139.00	1.36	0.69

Table 5
Self-measured compressive properties of produced materials along different orientations.

Material	Angle	Modulus [GPa]		Strength [MPa]		Strain to Failure [%]	
		Avg.	St. Dev.	Avg.	St. Dev.	Avg.	St. Dev.
DL-TS	0°	19.1	0.8	209.71	7.79	1.29	0.09
	90°	24.3	0.5	249.55	11.74	1.21	0.06
WL-TS	0°	20.3	0.5	226.32	10.21	1.30	0.16
	90°	16.8	0.6	233.58	11.08	1.62	0.07
DL-TP	0°	20.6	0.9	281.47	8.49	1.58	0.04
	90°	27.3	0.8	288.29	8.46	1.15	0.07
WL-TP	0°	26.0	0.4	357.84	10.52	1.57	0.07
	90°	20.6	1.9	311.31	31.42	1.66	0.05

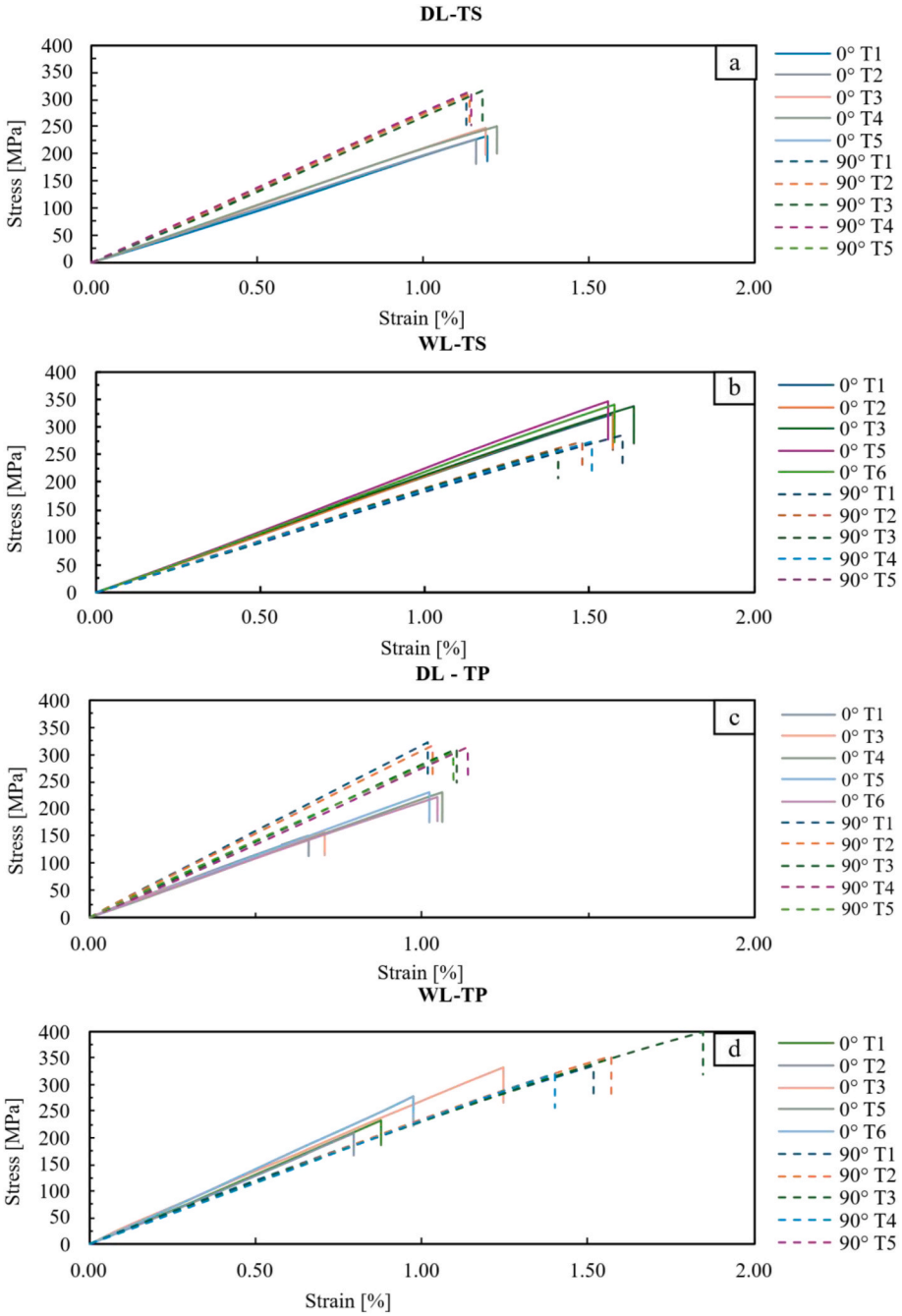

Fig. 9. Stress-strain curves from tensile tests (own measurements). a) DL-TS b) WL-TS c) DL-TP d) WL-TP.

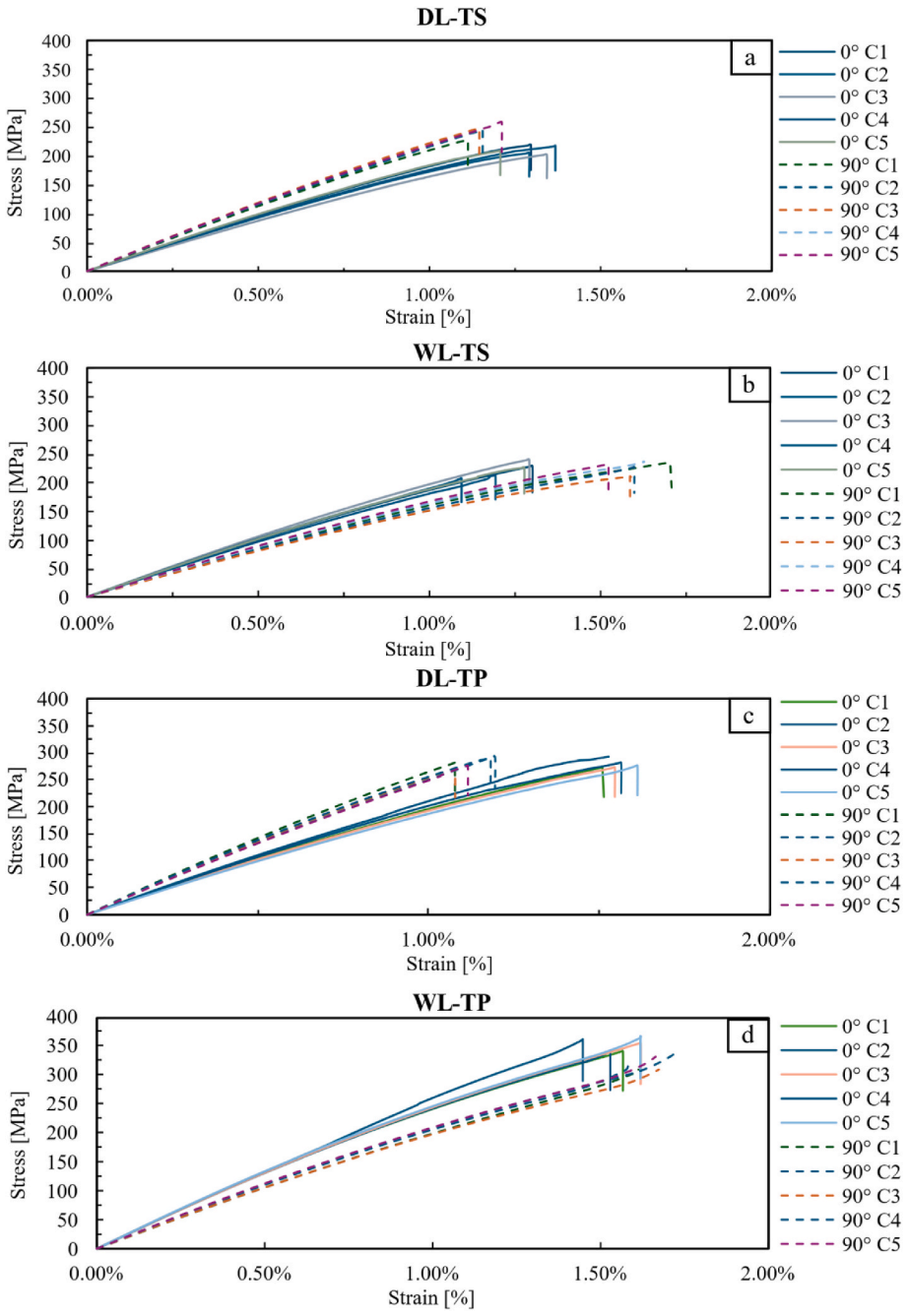

Fig. 10. Stress-strain curves from compressive tests (own research) a) DL-TS b) WL-TS c) DL-TP d) WL-TP.

higher compressive stiffness at 0° than at 90° orientation, with statistically significant differences ($p = 0.0031$ for WL-TP, $p < 0.00001$ for WL-TS). As the stress on a material increases, it transitions from linear elastic behavior to non-linear behavior, where it starts to strain harden. It can be argued that this change represents the point where the material begins to gradually fail. As visible in Fig. 10b and d, in WL-TS and WL-TP composites, the orientation at 0° demonstrates a higher threshold for stress before transitioning into a non-linear behavior phase. Conversely, DL-TS and DL-TP composites exhibit a superior stress resistance at the 90° orientation before entering the non-linear phase, as shown in Fig. 10a and c. Due to matrix ductility, the non-linear phase was more extended in DL-TP and WL-TP materials (Fig. 10c and d), particularly in the 90° orientation. The 0° orientation consistently achieves higher ultimate stress than the 90° orientation for DL-TS and DL-TP materials, indicating superior strength. It can be argued that this difference is caused by a preferential alignment of the fibers in the machine direction for the DL textile used, as observed in Section 3.1. After this peak, the materials experience failure, with a sharp drop in stress in brittle thermosets and a more gradual decline in ductile thermoplastics. The 90° orientation, although weaker in stress capacity, often shows higher strain at failure, meaning that it deforms more before breaking, particularly in WL-TP materials. In summary, each material shows adequate properties for short-fiber reinforced composites (S. J. Pickering et al., 2016; Zhao et al., 2018), and even surpasses conventional automotive materials made from virgin carbon fibers (Falaschetti et al., 2024).

3.2.3. *Flexural properties*

Results of the flexural test are given in Fig. 11 and summarized in Table 6.

For DL-TP and DL-TS materials, the stress-strain curves were linear

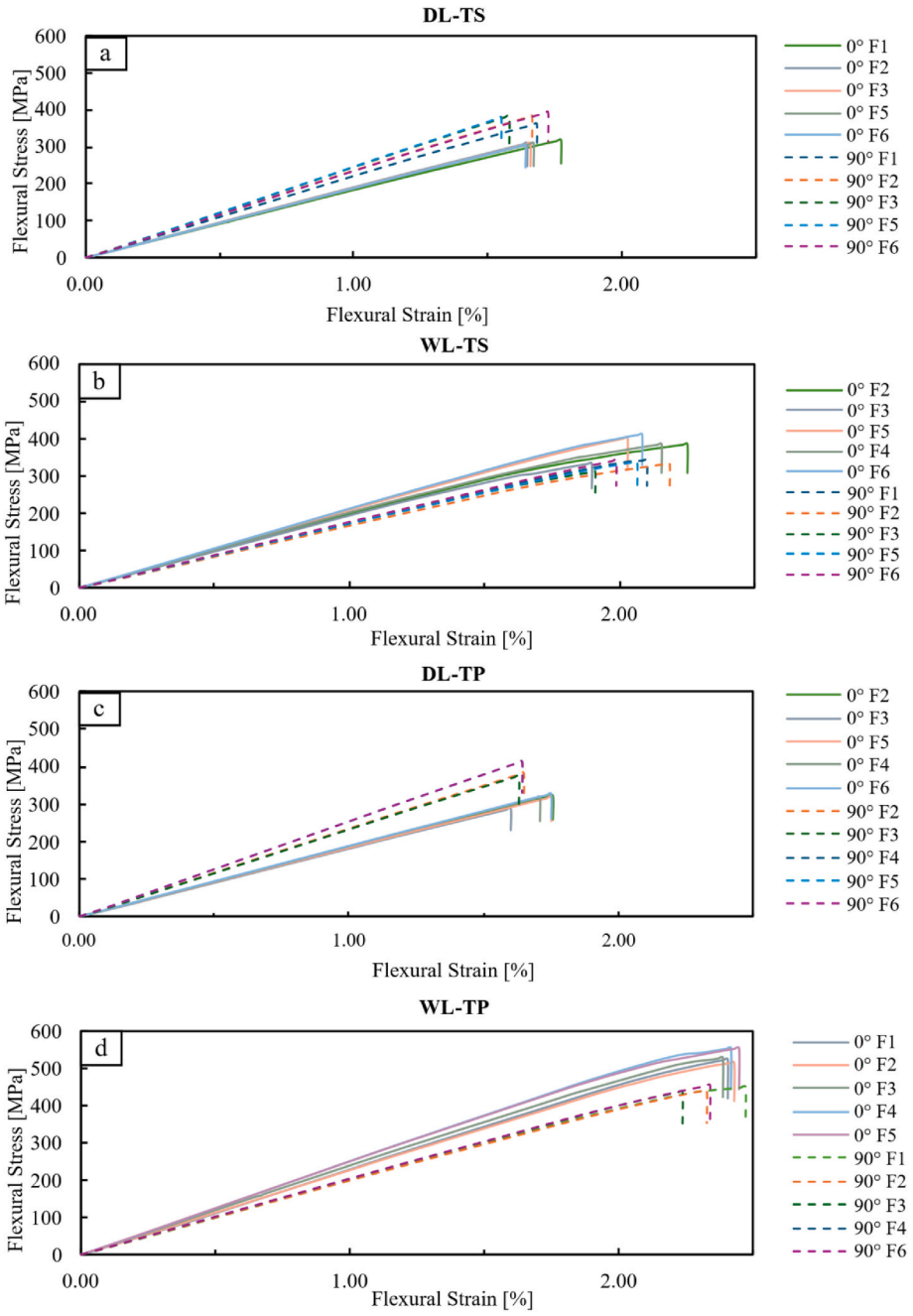

Fig. 11. Stress-strain curves from flexural tests (own research) a) DL-TS b) WL-TS c) DL-TP d) WL-TP.

Table 6
Self-measured flexural properties of produced materials along different orientations.

Material	Angle	Modulus [GPa]		Strength [MPa]		Strain to Failure [%]	
		Avg.	St. Dev.	Avg.	St. Dev.	Avg.	St. Dev.
DL-TS	0°	18.8	0.4	315.79	9.79	1.71	0.05
	90°	23.4	0.9	388.03	12.64	1.68	0.07
WL-TS	0°	19.8	0.9	376.62	35.79	2.10	0.12
	90°	16.9	0.5	332.75	17.88	2.10	0.11
DL-TP	0°	18.5	0.9	321.17	17.93	1.72	0.08
	90°	23.9	0.9	402.00	27.17	1.77	0.12
WL-TP	0°	22.9	1.8	532.58	26.98	2.46	0.05
	90°	19.9	0.4	455.24	7.82	2.41	0.13

up to failure (see Fig. 11a and c). In contrast, WL-TS and WL-TP materials showed an initial linear behavior, followed by a marked plastic region, ultimately terminating in abrupt failure (Fig. 11b and d). Different from what was observed in tensile, flexural curves are closely clustered, indicating high repeatability of the results. CV values for flexural modulus, ultimate stress, and strain at failure were consistently below 10 %, confirming the repeatability of the results. DL-TS and DL-TP materials still exhibit an anisotropic behavior, being stiffer in the cross direction (90°) than in the machine direction (0°), as a consequence of preferred fiber alignment in this direction. DL-TS and DL-TP exhibit comparable flexural properties at both 0° and 90°. The differences in modulus, strength, and strain to failure fall within experimental variability, showing no significant distinction between the two materials in flexural performance. Statistical analysis supports their similar mechanical behavior under bending loads. Both WL-TS and WL-TP showed

a less marked anisotropic behavior in flexure, as already observed in Section 3.1.1. and Section 3.1.2. with 0° orientation stiffer than 90°. Experimental evaluation confirmed these trends, with significant differences in flexural modulus ($p = 0.00058$ for WL-TS, $p = 0.00358$ for WL-TP). At a 0° orientation, WL-TP demonstrated the highest strength, with an average of 532.58 MPa and a range from 505.60 to 559.56 MPa, indicating its considerable consistency. In contrast, WL-TS presented a broader strength range (340.83–412.41 MPa), rendering it less reliable compared to DL-TS and DL-TP, which exhibited much narrower ranges (306.00–325.58 MPa and 303.24–339.10 MPa, respectively).

3.2.4. Comparison of all mechanical test results

Table 7 displays a summary of the results of all mechanical tests performed as well as the tendency in anisotropic behaviour of each material. All materials exhibit strong properties compared to other short-fiber reinforced composites and outperform conventional materials made with virgin carbon fibers in automotive applications. The most significant variance was found in DL-TP and WL-TP materials, which showed much higher stiffness in tension compared to compression, whereas DL-TS and WL-TS had higher tensile than compressive strength. Flexural modulus is slightly lower than tensile and compressive modulus on average, while flexural strength is higher than tensile and compressive strength. This supports the importance of fiber-matrix interaction in improving load-bearing conditions.

An assessment of the production processes studied could suggest that DL could be favourable due to low water consumption and high throughput, while WL has low dust emissions and mass loss (Karmakar et al., 2024; Ventura et al., 2022). The consolidation process for TP could have a higher environmental impact than for TS, due to the higher processing temperatures resulting in a higher energy consumption (Lunetto et al., 2023; Wegmann et al., 2022).

By comparing results in Table 8, for frame applications, WL-TP exhibited the most favourable profile, with high values across all indices: membrane stiffness (18.78–21.15 GPa cm^3/g), buckling resistance (11.42–14.44 $MPa^{0.5}\cdot cm^3/g$), and specific strength (170.98–273.16 MPa cm^3/g), consistently surpassing the commercial SMC benchmark. WL-TS also performed well, particularly in buckling resistance and specific strength, while DL-TP provided strong stiffness and strength despite a slightly lower buckling index. DL-TS, although the most limited, still matched or exceeded SMC in buckling and stiffness efficiency. These results confirm the potential of rCF laminates—especially WL variants—for structural applications.

The suitability of the rCF laminates for semi-structural panel applications was evaluated through Eq. (4), Eq. (5), and Eq. (6), which capture the primary mechanical demands placed on lightweight, thin-walled components such as roofs, hoods, and tailgates. Results of the analysis are illustrated in Table 9.

All laminates exhibited performance indices that were superior to the SMC reference. WL-TP stood out with the highest values across all three metrics, particularly in specific strength, reaching up to 407 MPa cm^3/g, and buckling stiffness, up to 3.65 $GPa^{1/2}\cdot cm^3/g$. These results reflect the improved load-carrying efficiency due to preferential in-plane fiber alignment. DL-TP and WL-TS also offered competitive performance, with bending stiffness efficiencies exceeding 2.1 $GPa^{1/3}\cdot cm^3/g$ and specific strengths well above 300 MPa cm^3/g. DL-TS remained comparable to or slightly better than SMC across all indices. Notably, the flexural properties, which dominate panel behaviour, benefit significantly from fiber orientation effects. This directional dependence contributes to the observed performance range and emphasizes the importance of manufacturing control, particularly in fiber alignment and dispersion. Despite these sensitivities, the results confirm that the rCF systems—especially WL-TP—are not only suitable replacements for conventional SMC but may also enable performance-driven improved lightweighting in exterior body components.

3.3. Fractographic analysis of tensile samples

The specimens subjected to tensile testing exhibited failure across multiple locations within the gauge length, suggesting that damage initiation and propagation occurred concurrently at several points. It can be argued that the material may have undergone localized stress concentrations or exhibited inherent weaknesses at various zones, leading to a simultaneous onset and propagation of damage rather than localized failure at a single point. Such behavior could be indicative of a material with uniform microstructural properties, or the presence of defects distributed throughout the specimen. When subjected to tensile loading, cracks initiate within the volume of the samples and propagate differently along the in-plane direction and through the thickness. Fig. 12 shows the typical failure of tensile specimens for the different materials tested.

In the in-plane direction, the fracture trajectory typically follows an approximately linear failure path, as shown in Fig. 12a–d. This often culminates in the detachment of material fragments, as observed in Fig. 12a and d. The debris released during testing was generally smaller in DL materials than in WL materials, indicating that textiles composed of shorter fibers tend to fragment more easily during failure. While this phenomenon can enhance the specific energy absorption in case of a crash event (Falaschetti et al., 2025), it can potentially limit fatigue performances (Mortazavian and Fatemi, 2015), and further investigations are needed. In contrast, when examining the samples in cross-section, the out-of-plane failure surface displayed a notably irregular and uneven topography. Through SEM investigations, a range of damage mechanisms has been elucidated, including fiber breakage, failure at the fiber-matrix interface (such as damage at fiber ends and debonding), and matrix cracking, as illustrated in Fig. 13.

DL-TS material exhibited an irregular fracture surface characterized by multiple fracture planes in the matrix. As shown in Fig. 13a, a significant proportion of the fibers are closely aligned with the fracture

Table 7
Comparison of the mechanical properties of all tested materials and their anisotropic behaviour.

Test type	Material	Strength [MPa]	Strength [MPa]	Stiffness [GPa]	Stiffness [GPa]	Anisotropy behaviour
		0°	90°	0°	90°	
Tensile	DL-TS	238.78	308.10	20.00	25.60	Higher properties in 90°, anisotropic tendency
	WL-TS	337.18	273.64	21.40	18.00	Mild anisotropy, stronger at 0°
	DL-TP	166.00	311.00	22.90	28.00	Higher properties in 90°, strong anisotropic behaviour
	WL-TP	223.99	275.99	27.70	24.60	Balanced, slightly stronger at 90°
Compressive	DL-TS	209.71	249.55	19.10	24.30	Anisotropic, stronger at 90°
	WL-TS	226.32	233.58	20.30	16.80	Preference for 90°
	DL-TP	281.47	288.29	20.60	27.30	High strength in both directions
	WL-TP	357.84	311.31	26.00	26.60	Mild anisotropy, stronger at 0°
Flexural	DL-TS	315.79	388.03	18.80	23.40	Maintain anisotropic characteristics
	WL-TS	376.62	332.75	19.80	16.90	less pronounced anisotropic behaviour
	DL-TP	321.17	402.00	18.50	23.90	Strong anisotropic behaviour
	WL-TP	532.58	455.24	22.90	19.90	Strong anisotropic behaviour, stronger in 0°

Table 8
Frame Selection Indices: Membrane stiffness efficiency, Buckling resistance efficiency, Specific strength.

Material	Membrane stiffness efficiency [GPa•cm^3/g]	Buckling resistance efficiency [MPa$^{0.5}$•cm^3/g]	Specific strength [MPa•cm^3/g]
DL-TS	15.27 ÷ 19.54	11.05 ÷ 13.40	160.08 ÷ 235.91
WL-TS	14.06 ÷ 16.72	11.75 ÷ 14.35	176.81 ÷ 263.42
DL-TP	17.48 ÷ 21.37	9.82 ÷ 13.47	126.39 ÷ 237.65
WL-TP	18.78 ÷ 21.15	11.4 ÷ 14.44	170.99 ÷ 273.16
SMC (Benchmark)	17.68 ÷ 21.87	10.13 ÷ 10.26	153.79 ÷ 157.84

Table 9
Panel parts selection indices: Bending Stiffness Efficiency, Buckling Stiffness Efficiency and Specific Strength.

Material	Bending Stiffness Efficiency [GPa$^{1/3}$•cm^3/g]	Buckling Stiffness Efficiency [GPa$^{1/2}$•cm^3/g]	Specific Strength [MPa•cm^3/g]
DL-TS	2.03 ÷ 2.18	3.31 ÷ 3.69	241 ÷ 246
WL-TS	2 ÷ 2.11	3.21 ÷ 3.48	260 ÷ 294
DL-TP	2.02 ÷ 2.2	3.28 ÷ 3.73	245 ÷ 307
WL-TP	2.07 ÷ 2.17	3.41 ÷ 3.65	348 ÷ 407
SMC (Benchmark)	1.89 ÷ 1.95	3.19 ÷ 3.33	234 ÷ 239

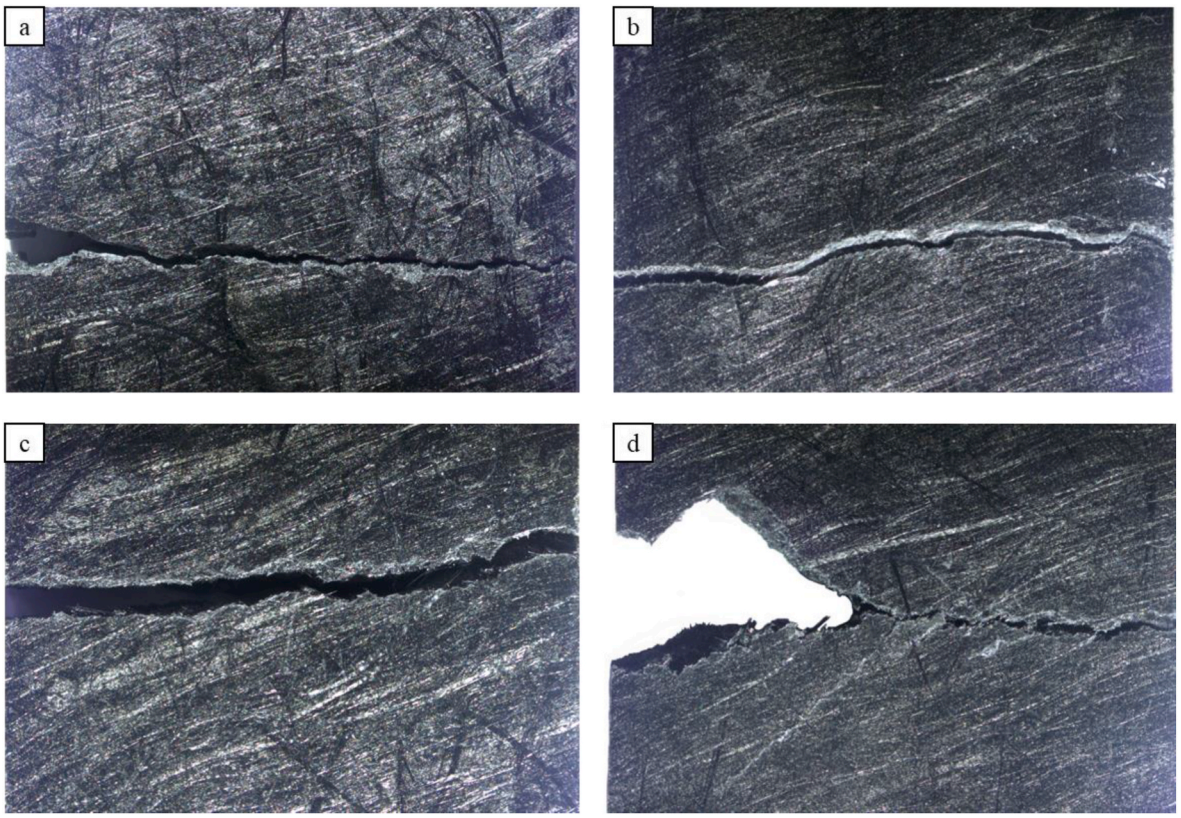

Fig. 12. Typical failure in tensile of a) DL-TS material b) WL-TS material c) DL-TP material d) WL-TP material.

plane, exhibiting a clean surface appearance. Additionally, there are several holes resulting from fibers that have been pulled out, which were approximately aligned with the direction of the primary load. The fracture surface of the surrounding matrix resin exhibited regions with well-defined hackle pattern features, typically terminating at an adjacent fiber end or a more extended detached fractured area. It can be argued that failure predominantly occurred by fiber-matrix debonding, with fiber ends acting as a trigger for crack initiation. The progression of damage in DL-TS materials appears to be highly influenced by the local distribution of fiber geometries, including orientations and configuration of surrounding fibers. These findings are in substantial agreement with observations noted in prior literature (Gao et al., 2024; Kimura et al., 2022; Rolland et al., 2017), underscoring the critical role of fiber-matrix debonding in the failure and fracture of short fiber composite. A representative micrograph of the fractured surface of the WL-TS material is shown in Fig. 13b. In this image, clusters of broken fibers and almost clean, pulled-out fibers are clearly visible. The surrounding matrix near the fibers appears smoother than the DL-TS material, with fewer rough fracture features or hackle patterns. This suggests that crack propagation in the WL-TS material occurred with minimal involvement of the polymer matrix, likely due to better compaction and a more uniform fiber distribution. This indicates that in WL-TS, the fibers dominate in determining the overall mechanical strength, with the matrix contributing less to fracture resistance. The cross-sectional fractured surfaces of DL-TP materials exhibit a highly irregular structure, with large areas of plastically deformed matrix surrounded by pulled-out or broken fibers (Fig. 13c). The fiber surfaces are consistently coated with significant traces of thermoplastic polymer,

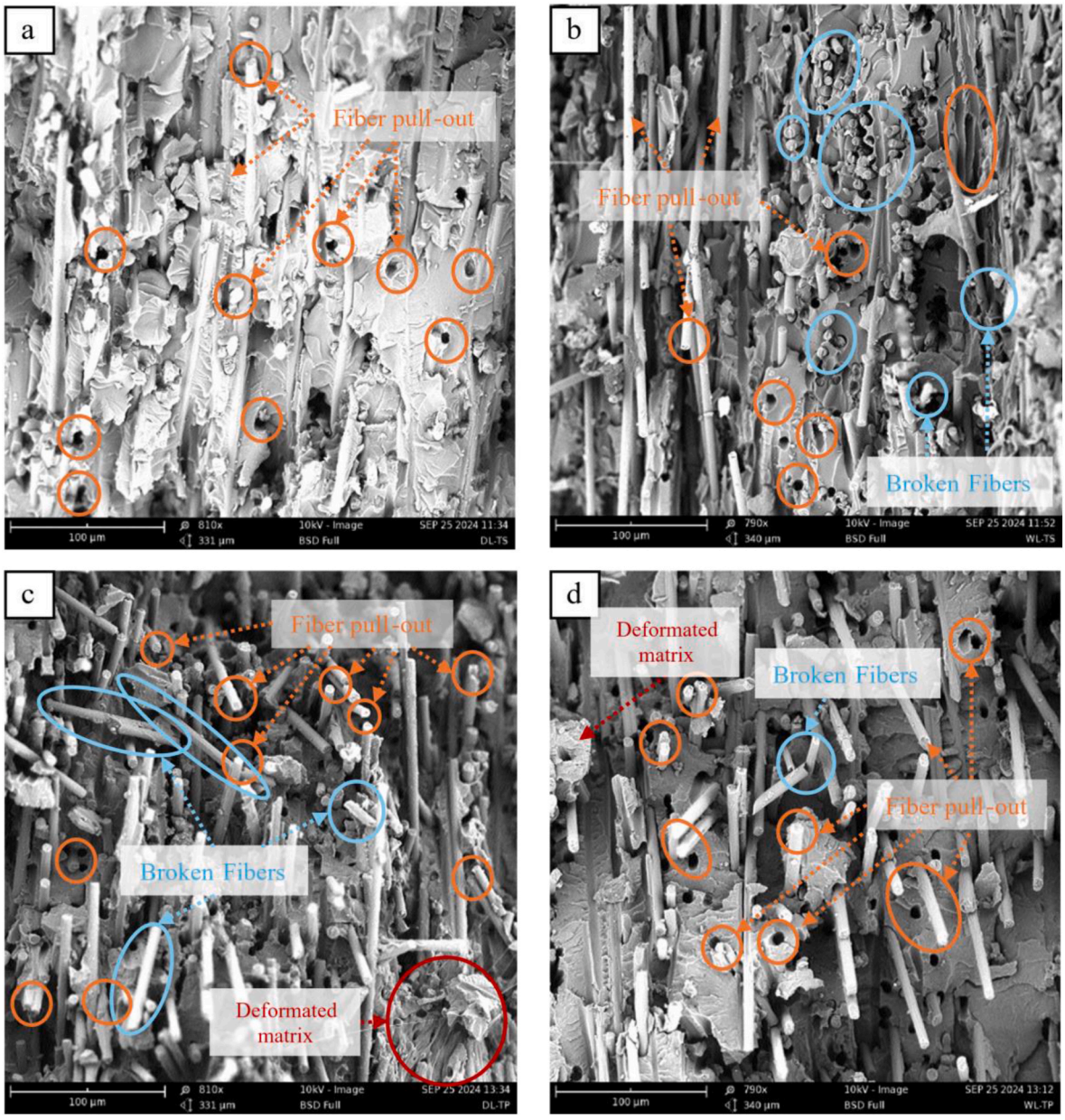

Fig. 13. Cross-section analysis of fractured surfaces of tensile samples at 0°. a) DL-TS material b) WL-TS material c) DL-TP material d) WL-TP material.

indicating strong adhesion between the matrix and the reinforcement. Broken fibers are visible as debris, typically ranging from 50 to 100 µm in length, as marked in Fig. 13c. This debris likely resulted from the fracturing process, as the critical fiber length of the reinforcement in the DL-TP material was significantly exceeded, preventing the fibers from being fully pulled out. This suggests that in DL-TP materials, the fibers dominate in determining the mechanical strength, while the matrix undergoes plastic deformation under loading. The fractured surfaces of WL-TP material exhibit a more regular topography than DL-TP materials. Fiber pull-out was consistently observed as the primary failure mechanism. As observed in DL-TP materials, the fibers are covered by debris of TP polymer, demonstrating an excellent adhesion between the matrix and the reinforcement. The fracture surface of the matrix is rough and exhibits visible hackle patterns, suggesting that the matrix experienced high deformation before breaking.

4. Conclusions and outlook

Four different material combinations with two nonwoven (DL and WL) and two polymer types (TS and TP) have been manufactured out of recycled carbon fibers with compression molding. The manufacturing aimed at a FVC of 30 %, and analysis shows that 23–28 % have been reached. Analysis from the microsection shows that TS material has more and larger voids than TP material, indicating potential higher mechanical properties in the TP material. The conclusions of the mechanical tests are the good and repeatable stiffness results (18–28 GPa) in all stress modes (tensile, compression and bending) and a higher performance of the DL-nonwovens material in cross direction due to production characteristics of the carding process. The WL-nonwovens demonstrate good and uniform stiffness results (16–26 GPa) and a more isotropic behaviour than DL. TP polymer provides generally better stiffness than the thermoset in the material combinations under investigation here, making it preferable in applications requiring a high stiffness. TS polymer presents stable and consistent data, but in general

less mechanical performance. In conclusion, this work provides insights in the mechanical performance of short-carbonfiber reinforced polymer composites and gives a better understanding of the material behavior. The material properties outperform standard short-fiber reinforced material and are therefore optimally suited for automotive applications (Falaschetti et al., 2024; K. L. Pickering et al., 2016; Zhao et al., 2018). Considering a potential recycling quota in the upcoming ELV directive, this material, using cut-off fibers from CFRP production scrap, provides a sustainable alternative to commercial FRPs. It should however be noted that the material investigated reaches similar material properties than quasi-isotropic glass or carbon fiber reinforced polymers, which are in general more cost effective in comparison (S. J. Pickering et al., 2016; Troiani et al., 2015). Further difficulties in industrialization of the process could include scalability issues in terms of product inconsistencies (fiber length, fiber sizing, etc.), the void management for TS-materials or the processing techniques. Future work should therefore focus on optimizing the manufacturing process to receive material with less voids, better fiber dispersion, a higher fiber volume content and consequently higher mechanical properties for a wider range of potential applications. Additionally, shear properties could not be determined due to the material structure and future research should therefore focus on working with thicker composites using the Iosipescu test method. Special attention should be paid to the environmental and economic assessment of the use of rCF as these results could increase the acceptance of the widespread use of the material.

CRediT authorship contribution statement

Fabian Rechsteiner: Writing – review & editing, Writing – original draft, Visualization, Supervision, Project administration, Methodology, Investigation, Formal analysis, Conceptualization. **Luca Raimondi:** Writing – review & editing, Writing – original draft, Visualization, Supervision, Methodology, Investigation, Formal analysis, Data curation. **Nicola Tegas:** Writing – original draft, Investigation, Data curation, Conceptualization. **Lorenzo Donati:** Validation, Supervision, Conceptualization. **Frank Manis:** Writing – review & editing, Methodology, Formal analysis, Conceptualization.

Data availability

The raw/processed data required to reproduce these findings cannot be shared at this time as the data also forms part of an ongoing study.

Funding

Luca Raimondi acknowledges the funding support of Ecosystem for Sustainable Transition in Emilia-Romagna Project, funded under the National Recovery and Resilience Plan (NRRP), Mission 04 Component 2 Investment 1.5—NextGenerationEU, call for tender n. 3277 dated December 30, 2021 Award Number: 0001052 dated June 23, 2022 CUP: B33D21019790006.

This research was financially supported by the German Federal Ministry of Economic Affairs and Climate Action through the German Federation of Industrial Research Associations (AiF) under the grant number 21793 (MAI ÖkoCaP).

Declaration of competing interest

The authors declare that they have no known competing financial interests or personal relationships that could have appeared to influence the work reported in this paper.

Acknowledgement

The authors would like to express their gratitude to **Asahi Kasei Corporation** for providing the thermoplastic material that was essential for the completion of this study. Their support greatly facilitated this research and contributed to the quality of the results presented in this paper.

Data availability

Data will be made available on request.

References

Ahmad, H., Markina, A.A., Porotnikov, M.V., Ahmad, F., 2020. A review of carbon fiber materials in automotive industry. In: IOP Conference Series: Materials Science and Engineering. https://doi.org/10.1088/1757-899X/971/3/032011.

Almushaikeh, A.M., Alaswad, S.O., Alsuhybani, M.S., AlOtaibi, B.M., Alarifi, I.M., Alqahtani, N.B., Aldosari, S.M., Alsaleh, S.S., Haidyrah, A.S., Alolyan, A.A., Alshammari, B.A., 2023. Manufacturing of carbon fiber reinforced thermoplastics and its recovery of carbon fiber: a review. Polym. Test. https://doi.org/10.1016/j.polymertesting.2023.108029.

Badrul Hasan, M.M., Nitsche, S., Abdkader, A., Cherif, C., 2019. Influence of process parameters on the tensile properties of DREF-3000 friction spun hybrid yarns consisting of waste staple carbon fiber for thermoplastic composites. Text. Res. J. 89, 32–42. https://doi.org/10.1177/0040517517736472.

Barnett, P.R., Ghossein, H.K., 2021. A review of recent developments in composites made of recycled carbon fiber textiles. Textiles 1, 433–465. https://doi.org/10.3390/textiles1030023.

Barnett, P.R., Young, S.A., Patel, N.J., Penumadu, D., 2021. Prediction of strength and modulus of discontinuous carbon fiber composites considering stochastic microstructure. Compos. Sci. Technol. 211. https://doi.org/10.1016/j.compscitech.2021.108857.

(BMW), L.B., 1999. Functional lightweight car bodies: the example of the new generation of BMW cars; Funktionaler Rohkarosserie-Leichtbau am Beispiel der neuen BMW-Generation. Stahl Eisen 119.

Cherif, C., 2011. Textile Werkstoffe Für Den Leichtbau - Techniken - Verfahren - Materialien -Eigenschaften. Springer Verlag.

Cui, X., Zhang, H., Wang, S., Zhang, L., Ko, J., 2011. Design of lightweight multi-material automotive bodies using new material performance indices of thin-walled beams for the material selection with crashworthiness consideration. Mater. Des. 32, 815–821. https://doi.org/10.1016/j.matdes.2010.07.018.

Danish, A., Mosaberpanah, M.A., Salim, M.U., Amran, M., Fediuk, R., Ozbakkaloglu, T., Rashid, M.F., 2022. Utilization of recycled carbon fiber reinforced polymer in cementitious composites: a critical review. J. Build. Eng. https://doi.org/10.1016/j.jobe.2022.104583.

Das, S., 2011. Life cycle assessment of carbon fiber-reinforced polymer composites. Int. J. Life Cycle Assess. 16, 268–282. https://doi.org/10.1007/s11367-011-0264-z.

David, F., Pizzi, E., Trovalusci, F., 2023. Investigation of the resin infusion process and mechanical performance of carbon fiber reinforced plastic composites from recycled carbon fiber. J. Compos. Mater. https://doi.org/10.1177/00219983231166892.

De Fazio, D., Boccarusso, L., Formisano, A., Viscusi, A., Durante, M., 2023. A review on the recycling technologies of fibre-reinforced plastic (FRP) materials used in industrial fields. J. Mar. Sci. Eng. https://doi.org/10.3390/jmse11040851.

Elmar, Witten, Mathes, Volker, 2022. Der Europäische Markt Für Faserverstärkte Kunststoffe/Composites 2021.

Falaschetti, M.P., Semprucci, F., Raimondi, L., Serradimigni, D., 2024. Experimental and numerical assessment of sheet molding compound composite crushing behavior. J. Mater. Eng. Perform. https://doi.org/10.1007/s11665-025-10833-2.

Falaschetti, M.P., Birnie Hernández, J., Semprucci, F., Raimondi, L., Serradimigni, D., Troiani, E., Donati, L., 2025a. Analysis of the Crushing Behavior of Flat Composite Plates Produced by Sheet Molding Compound. In: Dynamic Response and Failure of Composite Materials. Springer, pp. 40–48. https://doi.org/10.1007/978-3-031-77697-7_6.

Falaschetti, M.P., Semprucci, F., Birnie Hernández, J., Troiani, E., 2025. Experimental and numerical assessment of crashworthiness properties of composite materials: a review. Aerospace 12, 1–36. https://doi.org/10.3390/aerospace12020122.

Feraboli, P., Kawakami, H., Wade, B., Gasco, F., DeOto, L., Masini, A., 2012. Recyclability and reutilization of carbon fiber fabric/epoxy composites. J. Compos. Mater. 46, 1459–1473. https://doi.org/10.1177/0021998311420604.

Fu, S.Y., Lauke, B., Mai, Y.W., 2019. Science and engineering of short fibre-reinforced polymer composites. Science and Engineering of Short Fibre-Reinforced Polymer Composites. https://doi.org/10.1016/C2017-0-02431-X.

Gao, Q., Wan, Y., Wei, H., Takahashi, J., 2024. Characterization and prediction of tensile properties of carbon fiber-reinforced thermoplastics composed of hybrid short carbon fiber/PA6 fiber nonwoven mats. Compos. Struct. 334. https://doi.org/10.1016/j.compstruct.2024.117996.

Genna, S., Papa, I., Lopresto, V., Tagliaferri, V., 2020. Mechanical characterisation of CFRP laminates with recycled carbon fiber obtained by resin infusion under flexible tooling (RIFT) technology. Compos. Sci. Technol. 199. https://doi.org/10.1016/j.compscitech.2020.108328.

Gopalraj, S.K., Deviatkin, I., Horttanainen, M., Kärki, T., 2021. Life cycle assessment of a thermal recycling process as an alternative to existing cfrp and gfrp composite wastes management options. Polymers 13. https://doi.org/10.3390/polym13244430.

Handbuch Faserverbundkunststoffe/Composites, 2013. Handbuch faserverbundkunststoffe/composites. https://doi.org/10.1007/978-3-658-02755-1.

Heidarian, P., Mokhtari, F., Naebe, M., Henderson, L.C., Varley, R.J., 2024. Reclamation and reformatting of waste carbon fibers: a paradigm shift towards sustainable waste management. Resour. Conserv. Recycl. https://doi.org/10.1016/j.resconrec.2024.107465.

Henning, F., Moeller, E., 2020. Handbuch Leichtbau, Handbuch Leichtbau. Carl Hanser Verlag GmbH & Co. KG, München. https://doi.org/10.3139/9783446459847.fm.

Howarth, J., Mareddy, S.S.R., Mativenga, P.T., 2014. Energy intensity and environmental analysis of mechanical recycling of carbon fibre composite. J. Clean. Prod. 81, 46–50. https://doi.org/10.1016/j.jclepro.2014.06.023.

Hsissou, R., Seghiri, R., Benzekri, Z., Hilali, M., Rafik, M., Elharfi, A., 2021. Polymer composite materials: a comprehensive review. Compos. Struct. https://doi.org/10.1016/j.compstruct.2021.113640.

Iyer, K., Hagnell, M.K., Åkermo, M., 2024. The multi-objective optimization framework: a step towards minimizing life-cycle costs and energy consumption of carbon fibre automotive structures. Compos. Part B Eng. 271. https://doi.org/10.1016/j.compositesb.2023.111158.

Joost, W.J., 2012. Reducing vehicle weight and improving U.S. energy efficiency using integrated computational materials engineering. J. Occup. Med. 64, 1032–1038. https://doi.org/10.1007/s11837-012-0424-z.

Karmakar, S., Majumdar, A., Butola, B.S., 2024. A sustainable recycling process and its life cycle assessment for valorising post-consumer textile materials for thermal insulation applications. Waste Manag. Res. https://doi.org/10.1177/0734242X241270933.

Khurshid, M.F., Hengstermann, M., Hasan, M.M.B., Abdkader, A., Cherif, C., 2020. Recent developments in the processing of waste carbon fibre for thermoplastic composites – a review. J. Compos. Mater. https://doi.org/10.1177/0021998319886043.

Kim, H.H., Kim, B.J., 2023. Recovery of carbon fibers from carbon fiber-reinforced epoxy-isophorone diamine composites via step thermolysis. Compos. Part B Eng. 260. https://doi.org/10.1016/j.compositesb.2023.110757.

Kimura, M., Watanabe, T., Oshima, S., Takeichi, Y., Niwa, Y., Seryo, Y., Hojo, M., 2022. Nanoscale in situ observation of damage formation in carbon fiber/epoxy composites under mixed-mode loading using synchrotron radiation X-ray computed tomography. Compos. Sci. Technol. 230. https://doi.org/10.1016/j.compscitech.2022.109332.

Lunetto, V., Galati, M., Settineri, L., Iuliano, L., 2023. Sustainability in the manufacturing of composite materials: a literature review and directions for future research. J. Manuf. Process. https://doi.org/10.1016/j.jmapro.2022.12.020.

Manis, F., Stegschuster, G., Wölling, J., Schlichter, S., 2021. Influences on textile and mechanical properties of recycled carbon fiber nonwovens produced by carding. J. Compos. Sci. 5. https://doi.org/10.3390/jcs5080209.

Martulli, L.M., Creemers, T., Schöberl, E., Hale, N., Kerschbaum, M., Lomov, S.V., Swolfs, Y., 2020. A thick-walled sheet moulding compound automotive component: Manufacturing and performance. Compos. Part A Appl. Sci. Manuf. 128. https://doi.org/10.1016/j.compositesa.2019.105688.

Meng, F., McKechnie, J., Pickering, S.J., 2018. An assessment of financial viability of recycled carbon fibre in automotive applications. Compos. Part A Appl. Sci. Manuf. 109, 207–220. https://doi.org/10.1016/j.compositesa.2018.03.011.

Mortazavian, S., Fatemi, A., 2015. Fatigue behavior and modeling of short fiber reinforced polymer composites: a literature review. Int. J. Fatigue 70, 297–321. https://doi.org/10.1016/j.ijfatigue.2014.10.005.

Naqvi, S.R., Prabhakara, H.M., Bramer, E.A., Dierkes, W., Akkerman, R., Brem, G., 2018. A critical review on recycling of end-of-life carbon fibre/glass fibre reinforced composites waste using pyrolysis towards a circular economy. Resour. Conserv. Recycl. 136, 118–129. https://doi.org/10.1016/j.resconrec.2018.04.013.

Oliveux, G., Dandy, L.O., Leeke, G.A., 2015. Current status of recycling of fibre reinforced polymers: review of technologies, reuse and resulting properties. Prog. Mater. Sci. https://doi.org/10.1016/j.pmatsci.2015.01.004.

Pickering, K.L., Efendy, M.G.A., Le, T.M., 2016. A review of recent developments in natural fibre composites and their mechanical performance. Compos. Part A Appl. Sci. Manuf. https://doi.org/10.1016/j.compositesa.2015.08.038.

Pickering, S.J., Liu, Z., Turner, T.A., Wong, K.H., 2016. Applications for carbon fibre recovered from composites. In: IOP Conference Series: Materials Science and Engineering. https://doi.org/10.1088/1757-899X/139/1/012005.

Pimenta, S., Pinho, S.T., Robinson, P., Wong, K.H., Pickering, S.J., 2010. Mechanical analysis and toughening mechanisms of a multiphase recycled CFRP. Compos. Sci. Technol. 70, 1713–1725. https://doi.org/10.1016/j.compscitech.2010.06.017.

Prenzel, T.M., Hohmann, A., Prescher, T., Angerer, K., Wehner, D., Ilg, R., von Reden, T., Drechsler, K., Albrecht, S., 2024. Bringing light into the dark—overview of environmental impacts of carbon fiber production and potential levers for reduction. Polymers 16. https://doi.org/10.3390/polym16010012.

Raimondi, L., Brugo, T.M., Zucchelli, A., 2021. Fiber misalignment analysis in PCM-UD composite materials by full field nodal method. Compos. Part C Open Access 5. https://doi.org/10.1016/j.jcomc.2021.100151.

Rietveld, T., van Hout, R., 2015. The t test and beyond: recommendations for testing the central tendencies of two independent samples in research on speech, language and hearing pathology. J. Commun. Disord. 58, 158–168. https://doi.org/10.1016/j.jcomdis.2015.08.002.

Rimmel, O., May, D., Goergen, C., Poeppel, A., Mitschang, P., 2019. Development and validation of recycled carbon fiber-based binder tapes for automated tape laying processes. J. Compos. Mater. 53, 3257–3268. https://doi.org/10.1177/0021998318820422.

Rolland, H., Saintier, N., Wilson, P., Merzeau, J., Robert, G., 2017. In situ X-ray tomography investigation on damage mechanisms in short glass fibre reinforced thermoplastics: effects of fibre orientation and relative humidity. Compos. Part B Eng. 109, 170–186. https://doi.org/10.1016/j.compositesb.2016.10.043.

Sauer, M., Feil, J., Manis, F., Betz, T., Drechsler, K., 2019. Thermoplastic multi-material nonwovens from recycled carbon fibres using wet-laying technology. In: Key Engineering Materials, pp. 210–216. https://doi.org/10.4028/www.scientific.net/KEM.809.210.

Seabold, S., Perktold, J., 2010. Statsmodels: econometric and statistical modeling with python. In: Proceedings of the 9th Python in Science Conference, pp. 92–96. https://doi.org/10.25080/majora-92bf1922-011.

Shah, D.U., Schubel, P.J., 2016. On recycled carbon fibre composites manufactured through a liquid composite moulding process. J. Reinf. Plast. Compos. 35, 533–540. https://doi.org/10.1177/0731684415623652.

Shen, Y., Apraku, S.E., Zhu, Y., 2023. Recycling and recovery of fiber-reinforced polymer composites for end-of-life wind turbine blade management. Green Chem. https://doi.org/10.1039/d3gc03479h.

Sun, D., Tao, C., 2018. Lightweight study of carbon fiber composite B-Pillar based on equal stiffness principle. OALib 5, 1–12. https://doi.org/10.4236/oalib.1104822.

Troiani, E., Falaschetti, M.P., Taddia, S., Ceruti, A., 2015. CFRP crash absorbers in small UAV: design and optimization. In: SAE Technical Papers. https://doi.org/10.4271/2015-01-2461.

Ventura, H., Álvarez, M.D., Gonzalez-Lopez, L., Claramunt, J., Ardanuy, M., 2022. Cement composite plates reinforced with nonwoven fabrics from technical textile waste fibres: mechanical and environmental assessment. J. Clean. Prod. 372. https://doi.org/10.1016/j.jclepro.2022.133652.

Vo Dong, P.A., Azzaro-Pantel, C., Cadene, A.L., 2018. Economic and environmental assessment of recovery and disposal pathways for CFRP waste management. Resour. Conserv. Recycl. 133, 63–75. https://doi.org/10.1016/j.resconrec.2018.01.024.

Wan, Y., Takahashi, J., 2016. Tensile properties and aspect ratio simulation of transversely isotropic discontinuous carbon fiber reinforced thermoplastics. Compos. Sci. Technol. 137, 167–176. https://doi.org/10.1016/j.compscitech.2016.10.024.

Wegmann, S., Rytka, C., Diaz-Rodenas, M., Werlen, V., Schneeberger, C., Ermanni, P., Caglar, B., Gomez, C., Michaud, V., 2022. A life cycle analysis of novel lightweight composite processes: reducing the environmental footprint of automotive structures. J. Clean. Prod. 330. https://doi.org/10.1016/j.jclepro.2021.129808.

Witik, R.A., Teuscher, R., Michaud, V., Ludwig, C., Månson, J.A.E., 2013. Carbon fibre reinforced composite waste: an environmental assessment of recycling, energy recovery and landfilling. Compos. Part A Appl. Sci. Manuf. 49, 89–99. https://doi.org/10.1016/j.compositesa.2013.02.009.

Wölling, J., Schmieg, M., Manis, F., Drechsler, K., 2017. Nonwovens from recycled carbon fibres - comparison of processing technologies. In: Procedia CIRP, pp. 271–276. https://doi.org/10.1016/j.procir.2017.03.281.

Wong, K.H., Turner, T.A., Pickering, S.J., 2014. Challenges in developing nylon composites commingledwith discontinuous recycled carbon fibre. In: 16th European Conference on Composite Materials. ECCM 2014.

Xiao, B., Zaima, T., Shindo, K., Kohira, T., Morisawa, J., Wan, Y., Yin, G., Ohsawa, I., Takahashi, J., 2019. Characterization and elastic property modeling of discontinuous carbon fiber reinforced thermoplastics prepared by a carding and stretching system using treated carbon fibers. Compos. Part A Appl. Sci. Manuf. 126. https://doi.org/10.1016/j.compositesa.2019.105598.

Yurgartis, S.W., 1987. Measurement of small angle fiber misalignments in continuous fiber composites. Compos. Sci. Technol. 30, 279–293. https://doi.org/10.1016/0266-3538(87)90016-9.

Zhao, G., Zhong, J., Zhang, Y.X., 2018. Research progress on mechanical properties of short carbon fibre/epoxy composites. Recent Patents Mech. Eng. 12, 3–13. https://doi.org/10.2174/2212797612666181213091233.

Zweifel, L., Brauner, C., 2020. Investigation of the interphase mechanisms and welding behaviour of fast-curing epoxy based composites with co-cured thermoplastic boundary layers. Compos. Part A Appl. Sci. Manuf. 139. https://doi.org/10.1016/j.compositesa.2020.106120.